Journal of
Marine Science and Engineering

MDPI

Article

Results of the Study of Resonant Oscillations in the Northern Part of the Shelf of the Peter the Great Gulf, the Sea of Japan

Sergey Smirnov [1], Grigory Dolgikh [2], Igor Yaroshchuk [2], Alexander Lazaryuk [2], Alexandra Kosheleva [2,*], Alex Shvyrev [2], Alexander Pivovarov [2] and Aleksandr Samchenko [2]

[1] Institute of Automation and Control Processes, Far Eastern Branch Russian Academy of Sciences, 690041 Vladivostok, Russia; smirnoff@iacp.dvo.ru

[2] V.I. Il'ichev Pacific Oceanological Institute, Far Eastern Branch Russian Academy of Sciences, 690041 Vladivostok, Russia; dolgikh@poi.dvo.ru (G.D.); yaroshchuk@poi.dvo.ru (I.Y.); lazaryuk@poi.dvo.ru (A.L.); shvyrev@poi.dvo.ru (A.S.); pivovarov@poi.dvo.ru (A.P.); samchenko.an@poi.dvo.ru (A.S.)

* Correspondence: kosheleva@poi.dvo.ru

Abstract: To study the features of resonant oscillations in the water column of the Peter the Great Gulf of the Sea of Japan, in situ measurements were carried out on its shelf, combined with numerical simulation of these processes. The observational data were obtained from autonomous bottom pressure gauges in Novik Bay in the winter of 2016. In the calculations, a spectral-difference model was used, modified to account for the ice cover, and implemented on an irregular triangular grid. The atmospheric forcing used in the model had periods from 15 to 55 min. As a result, characteristic series of spatio-temporal parameters for resonant oscillations of the studied water area were determined. The locations of the peaks on the simulated resonance curves correspond to the locations of well-defined maxima of the energy spectrum according to in situ measurements, hence indicating the possibility of a significant resonant amplification of level fluctuations by wave and periodic wind effects. The novelty of this study is inclusion of the winter period, when the surface of the bay is partially covered with ice.

Keywords: resonant oscillations; seiches; Peter the Great Gulf; spectral analysis; numerical model

Citation: Smirnov, S.; Dolgikh, G.; Yaroshchuk, I.; Lazaryuk, A.; Kosheleva, A.; Shvyrev, A.; Pivovarov, A.; Samchenko, A. Results of the Study of Resonant Oscillations in the Northern Part of the Shelf of the Peter the Great Gulf, the Sea of Japan. *J. Mar. Sci. Eng.* **2023**, *11*, 1973. https://doi.org/10.3390/jmse11101973

Academic Editor: Jean-Louis Pinault

Received: 30 August 2023
Revised: 24 September 2023
Accepted: 27 September 2023
Published: 12 October 2023

1. Introduction

Currently, research on natural phenomena that pose a threat to populations and various structures in coastal zones remains relevant [1]. These natural hazards include tsunamis, meteotsunamis, strong seiches, and storm surges. In each region, these phenomena have their own characteristics and require separate research. This partly explains the constant growth of publications on the subject. As an example, we mention relatively recent reviews of tsunami studies [2,3] and meteotsunamis [4]. Large-amplitude seiche oscillations accompanied by flooding of coastal areas can be interpreted as one of the meteotsunami types [5]. Regional characteristics must be taken into account when studying the wave interactions of coastal waters with a sea or ocean. For example, there may be some peculiar features of the bottom topography [6] or reefs [7] between coastal waters and the sea. The task becomes more complicated if the coastal water area is located in a bay and does not directly border the sea. In this case, it is necessary to study and consider the resonant properties of the bay. The problem becomes even more complicated when there are several bays or seas, as is the case of the Mediterranean Sea. In this case, a complex oscillatory system becomes the subject of study. In coastal waters, for example, tidal resonant oscillations of adjacent waters can be observed [8].

The subject of this work is to study resonant oscillations in the Peter the Great Gulf of the Sea of Japan. The water area of the gulf is exposed to the hazards of wave action of seismic and meteorological origin [9]. The bottom topography of the northern part of the shelf of the Peter the Great Gulf of the Sea of Japan is shown in Figure 1. An important component of the resonant oscillations study is the use of numerical modeling, which allows us to reveal the spatial form of oscillations recorded at measuring stations. Knowledge of the spatial structure of resonant oscillations makes it possible to determine areas of the coast that are prone to flooding.

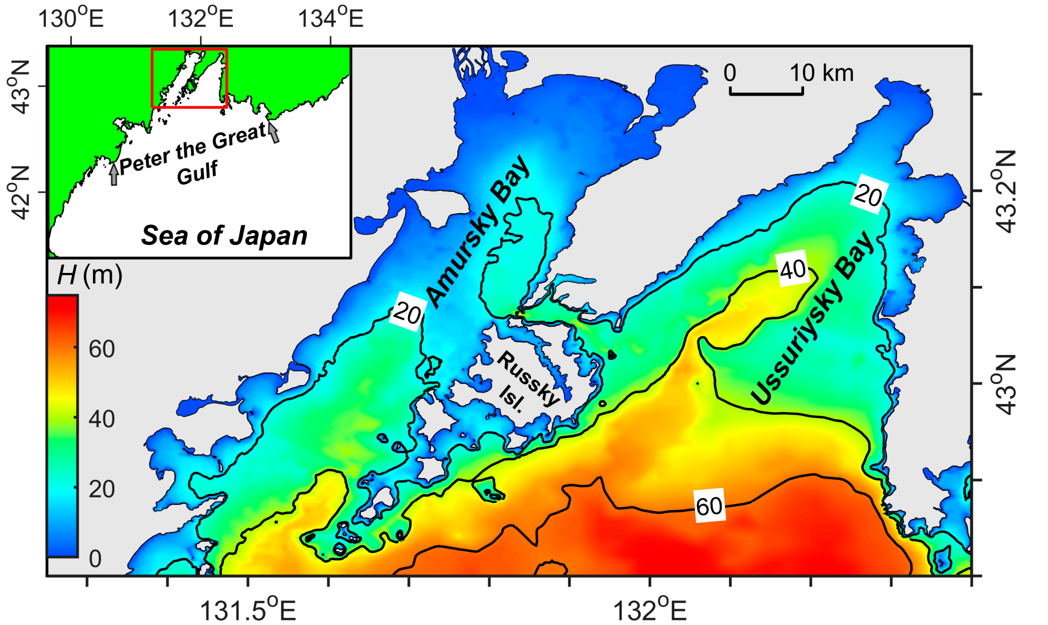

Figure 1. Bottom topography of the northern part of the shelf of the Peter the Great Gulf of the Sea of Japan. Isobaths are shown at intervals of 20 m. Insert: general view of the Peter the Great Gulf; grey arrows mark the boundaries of the gulf.

The Peter the Great Gulf is a complex oscillatory system connected by a wide entrance with the Sea of Japan. Previous studies [10–15] considered resonant oscillations in the Peter the Great Gulf without ice cover. In this paper, we consider resonant oscillations in the winter period, when the surface of the gulf is partially covered with ice.

One of the components of the oscillatory system of the northern part of the Peter the Great Gulf shelf is Novik Bay. Novik Bay cuts deep into the northwestern part of Russky Island, has length of more than 12 km, an area of 12.7 km^2, and a maximum width of about 2 km. Its depth reaches 20 m between the entrance capes. The Novik Bay water area has been an intracity water body of Vladivostok since 1991; nevertheless, it remains the least studied. The bottom topography of Novik Bay is shown in Figure 2. Figures 1 and 2 do not show isobaths in areas with abrupt changes in depth, where the distance between isolines is less than the thickness of the curves.

The quiet and calm Novik Bay usually freezes by mid-December, freeing itself from ice in early April. During this period, its waters, as a rule, are colder and saltier than in the adjacent Amursky Bay, due to the shallow water and brine released during ice formation. As a result, during freeze-up, due to the spatial density gradient, a flow of highly saline waters forms in the near-bottom layer, directed northward to the exit from the bay [16].

To study the features of resonant oscillations in the water column of the Peter the Great Gulf, the staff of the Pacific Oceanological Institute of the Far Eastern Branch of Russian Academy of Sciences (POI FEB RAS) conducted in situ measurements on the shelf of the gulf in the winter of 2016, with the installation of autonomous pressure gauges in Novik Bay. Interpretation and joint analyses of the measurement results were performed using the spatio-temporal parameters of resonant oscillations obtained at the Institute of Automation and Control Processes (IACP FEB RAS) using a numerical model.

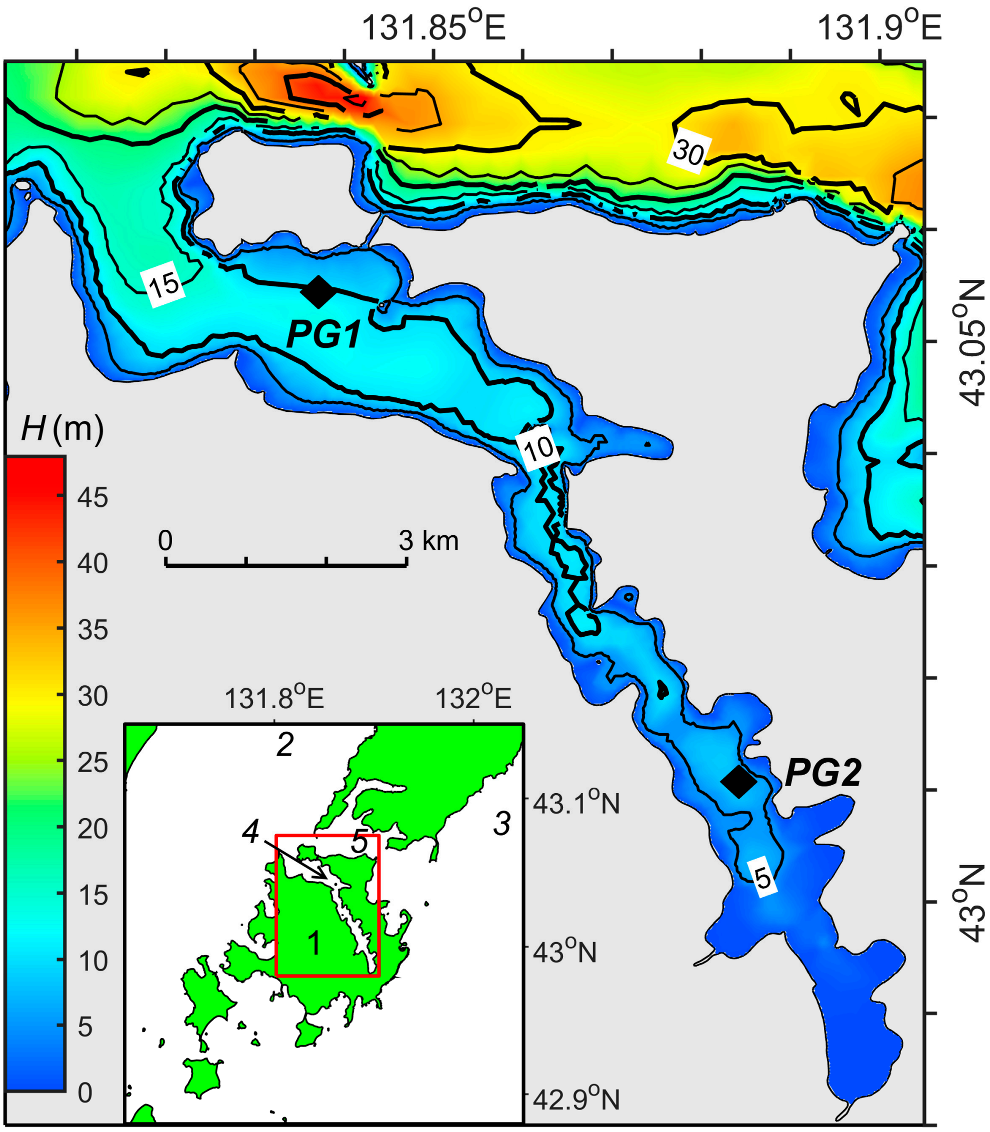

Figure 2. Bottom topography of Novik Bay of the Peter the Great Gulf. The isobaths are shown at intervals of 5 m. Symbol ♦ shows the position of the autonomous bottom pressure gauges PG1 and PG2. The digits in insert indicate: 1—Russky Island; 2—Amursky Bay; 3—Ussuriysky Bay; 4—Novik Bay; 5—the Eastern Bosphorus Strait.

2. Materials and Methods

2.1. In Situ Measurements

Field studies of spatio-temporal variability of the surface level of Novik Bay (Russky Island), covered with a solid ice field, continued from 30 January to 15 March 2016. We used two autonomous bottom gauges (loggers) of hydrostatic pressure [17]. The first instrument was installed at a depth of about 14.5 m at the point with coordinates 43°03.27′ N, 131°50.2′ E, and the second (8.7 m) at 43°00.644′ N, 131°53.05′ E. (Figure 2). At the time of their installation/removal, the ice cover had thickness of about 28/43 cm and 41/64 cm, respectively.

Data from the weather station WMO_ID = 31,960 (Vladivostok, the Archive of the Primorsky Department of Hydrometeorology and Environmental Monitoring, http://rp5.ru; accessed on 29 August 2023) showed about 46 mm of precipitation within the specified period, an average air temperature of about −7 °C, and variations in its average daily values from −18 °C to +2.5 °C. At the same time, the average values of the thermohaline characteristics of the under-ice water column measured by an autonomous CTD profiler in Novik Bay were in the range of −1.83 °C to −1.07 °C and from 33.82 psu to 34.37 psu.

The gauges used thermally stabilized strain gauge transducers D0.4-T with the maximum immersion depth of 40 m, sampling frequency of 10 Hz, and resolution of 0.01%, which corresponds to 4 mm of water column [17].

When performing the analysis of oscillations from in situ measurements data, the spectral analysis described in [18] was used.

2.2. Spectral-Difference Model

To calculate the forced oscillations, we used a modified spectral-difference model [11], incorporating terms into the equations to account for ice effects. We assume the ice cover to be absolutely flexible and smooth, and the points of its middle surface move only vertically. The model is based on the system of linearized depth-averaged equations of motion and continuity, written in spherical coordinates [19] (p. 596), in which components of the wind stress are local in space and periodic in time, with frequency σ. Horizontal turbulent exchange is not taken into account; bottom friction force is described by a linear dependence on the velocity components with a coefficient r_B:

$$\frac{\partial u}{\partial t} - fv = -\frac{g}{a\cos\phi}\frac{\partial \zeta}{\partial \lambda} - \frac{r_B}{\max(H, H_B)}u + I_{\text{ice}}\frac{A_\tau B(r)}{\rho_0 H}\cos\sigma t \sin\theta_\tau, \tag{1}$$

$$\frac{\partial v}{\partial t} + fu = -\frac{g}{a}\frac{\partial \zeta}{\partial \phi} - \frac{r_B}{\max(H, H_B)}v + I_{\text{ice}}\frac{A_\tau B(r)}{\rho_0 H}\cos\sigma t \cos\theta_\tau, \tag{2}$$

$$\frac{\partial \zeta}{\partial t} + \frac{1}{a\cos\phi}\left(\frac{\partial Hu}{\partial \lambda} + \frac{\partial Hv\cos\phi}{\partial \phi}\right) = 0, \tag{3}$$

$$H = H_{\text{bathymetry}} + h_{\text{corr}} - h_{\text{ice}}\frac{\rho_{\text{ice}}}{\rho_0}, \tag{4}$$

$$B(r) = \begin{cases} 1, & r \le r_1, \\ \frac{1}{2}\cos\pi\frac{r-r_1}{r_0-r_1} + \frac{1}{2}, & r_1 < r < r_0 \\ 0, & r \ge r_0 \end{cases}, \quad r \equiv r(\lambda, \phi; \lambda_\tau, \phi_\tau), \tag{5}$$

where a is mean radius of the Earth; λ and ϕ are geographic longitude and latitude; t is time; g is gravity acceleration; u and v are components of the velocity vector by directions λ and ϕ, respectively; ζ is elevation of the free surface above the undisturbed position; ρ_0 is characteristic density of water; ρ_{ice} is characteristic ice density; H is thickness of the undisturbed liquid layer; h_{ice} is ice thickness; H_B is thickness of the near-bottom boundary layer; $H_{\text{bathymetry}}$ is depth from navigation charts and data bases; $f = 2\omega\sin\phi$ is Coriolis parameter; ω is angular speed of rotation of the Earth; θ_τ is azimuth of wind action direction; A_τ is the maximum amplitude of wind stress; λ_τ and ϕ_τ are coordinates of the center of the wind forcing area; r is the distance between points (λ,ϕ) and (λ_τ,ϕ_τ); $I_{\text{ice}} = 0$ in the presence of ice; $I_{\text{ice}} = 1$ in ice-free water area; and h_{corr} is depth correction. The h_{corr} variable denotes a group of terms with periods longer than one day, describing the contribution of long-period tides, wind surges, atmospheric pressure, water exchange through straits, and also compensating for errors in bathymetry data and ice thickness values. An "impermeable" boundary condition is specified at the solid vertical boundary. A radiation condition is set at the liquid vertical boundary [19] (p. 598).

The numerical solution of system (1)–(5) is sought in the form of steady forced oscillations with frequency σ. We employ the widely recognized transition to complex variables, which is described, for example, in [13]. Difference analogs for the original differential equations are constructed in accordance with [20] (3.2.1. The 2-D External Mode, 3.5. Finite-Volume Discrete Methods in Spherical Coordinate System). To solve the resulting system of linear algebraic equations, the SuperLU MT 3.0 linear algebra package [21] is used.

To construct the $H_{\text{bathymetry}}$ model bottom topography, we employed navigation charts [22] in the coastal area and GEBCO 2020 [23] data for the rest of the water area. The technique for constructing the irregular triangular grid is described in [14]. The dimensions of the grid triangles of the model water area are determined by the depth values. The length of the side of the smallest triangle Δ_0 = 51 m. These triangles are used at depths greater than H_0 = 0.317 m. The lengths of sides of the triangles, ranked by size, are progressively doubled step by step: $\Delta_n = \Delta_0 \times 2^n$, where $n = 0, \ldots, 6$. Triangles with a side length Δ_n are employed for water areas with depths exceeding $H_n = H_0 \times 2^{2n}$. The largest triangles, with a side length Δ_6 = 3264 m, are used for water areas with depths exceeding H_6 = 1300 m. Figure 3 shows a fragment of the model grid for the Novik Bay water area; the insert shows the entire grid area.

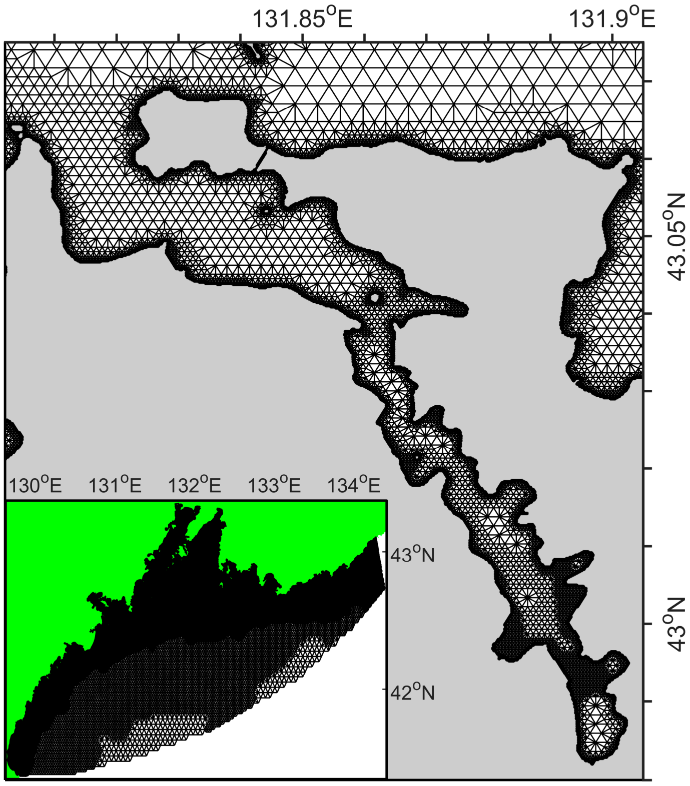

Figure 3. Irregular triangular grid of the model water area of Novik Bay. Land is shown in grey. Insert: grid for the entire computational domain. Land is shown in green.

Let us evaluate the influence of grid resolution on the spectral properties of grid waves. the frequency equations for one-dimensional gravity-inertia waves in the continuous case are as follows [24] (Equation (3.4) p. 48):

$$\sigma^2 = f^2 + gHk^2, \ \ \sigma = \frac{2\pi}{T}, \tag{6}$$

and, for gravity-inertia waves on the grid of type (B) [24] (Equation $(3.6)_\mathrm{B}$ p. 49):

$$\sigma_\mathrm{m}{}^2 = f^2 + \frac{4gH}{d^2}\sin^2\frac{kd}{2}, \ \ \sigma_\mathrm{m} = \frac{2\pi}{T_\mathrm{m}}, \tag{7}$$

where k is the wave number, d is the grid step, and σ_m and T_m are the frequency and period of the grid wave. In the approximation of high grid resolution, Equation (7) can be presented in the following simplified form:

$$\sigma_\mathrm{m}{}^2 \approx f^2 + gHk^2 - \frac{gH}{12}k^4d^2 \quad (kd \ll 1). \tag{8}$$

Let us denote the relative deviation of the frequency of the grid solution by variable ε

$$\varepsilon = \frac{\sigma - \sigma_{\mathrm{m}}}{\sigma} \ll 1, \tag{9}$$

and exclude the variables k and σ_{m} from the system of Equations (6)–(9). We obtain

$$d^2\,\sigma^4 - \left(24gH\varepsilon + 2f^2d^2\right)\sigma^2 + d^2f^4 = 0. \tag{10}$$

Let us consider the case when the frequency is much higher than the inertial frequency. In this, approximation (10) is significantly simplified

$$d^2\,\sigma^2 - 24gH\varepsilon\ = 0\ \ (\sigma \gg f). \tag{11}$$

Let $T = T_*$, $d = d_*$, $H \geq H_*$ and

$$\varepsilon_* = \frac{\pi^2}{6g}\frac{{d_*}^2}{H_*{T_*}^2} \tag{12}$$

then the inequality $\varepsilon \leq \varepsilon_*$ is true. When assessing the properties of waves on the triangular grid in Equations (10)–(12), the grid step should be replaced by the longest side length of the triangle. Let us substitute into (11) $H_* = H_0 \times 2^{2n}$, $d_* = \Delta_0 \times 2^n$, $H_0 = 0.317$ m, $\Delta_0 = 51$ m. At $T_* = 60$ min, we obtain $\varepsilon_* \approx 0.0001$; at $T_* = 15$ min, we obtain $\varepsilon_* \approx 0.0017$. These values indicate the limits of the range of the upper estimate of the relative deviation of the grid waves frequencies considered in this work.

For the water area of Novik Bay h_{ice}, the ice thickness is set equal to 44 cm (the average value for the observation period of 2016). Figure 4 shows two variants of the configuration of the ice cover of the model area. The variant shown in Figure 4a is the main one. The contours of the distribution of the ice cover thickness approximately correspond to the satellite image from the site https://www.dvrcpod.ru/News.php?id_new=1686; accessed on 29 August 2023, and the ice thicknesses are set by the characteristic values of 11, 33, and 55 cm. Figure 4b shows the auxiliary variant with constant ice thickness of 22 cm.

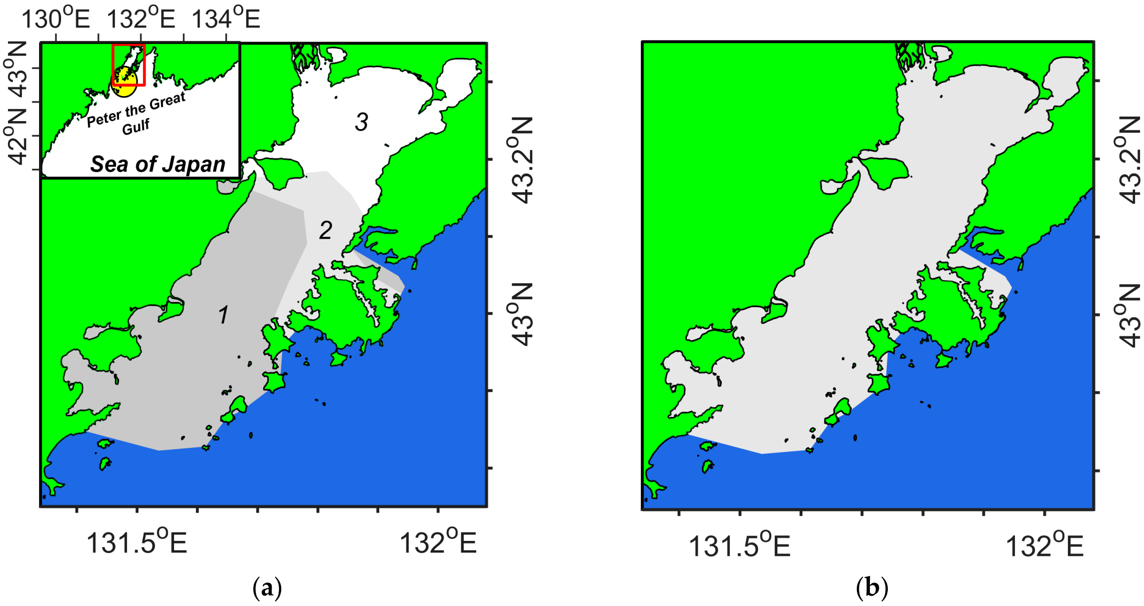

Figure 4. Two variants of ice thickness distribution in the model water area of the Peter the Great Gulf. The land is shown in green, the ice is gray, and the rest of the water area is blue. (**a**) Areas with ice thickness of 11, 33, and 55 cm are labeled 1, 2, and 3, respectively. The insert shows the area of wind forcing in yellow. (**b**) Ice with uniform thickness of 22 cm.

Numerical solutions were obtained for the following variant of wind forcing. The amplitude of the driving force was set equal to zero outside the circle of radius r_0 = 25 km, and a constant value inside the circle of radius r_1 = 20 km. The coordinates of the center of the wind effect area were set as $(\lambda_\tau; \phi_\tau)$ = (131.6° E, 42.8° N). The location of the area of the model wind forcing is shown in the insert in Figure 4. In the numerical model, the coefficients $r_B = 1.5 \times 10^{-5}$ m/s, H_B = 2 m, and the characteristic density values were set as $\rho_0 = 1028$ kg/m^3, $\rho_{\text{ice}} = 927$ kg/m^3. For each given value of σ, solutions are calculated for northern ($\theta_\tau = 0$) and eastern ($\theta_\tau = \pi/2$) directions. A linear combination of these two solutions with multipliers $\cos\theta_\tau$ and $\sin\theta_\tau$, respectively, corresponds to the direction with an arbitrary θ_τ.

3. Results

3.1. In Situ Measurements

Figure 5a,b and Figure 6a,b show non-averaged spectral estimations at stations PG1 and PG2 for the range of periods from 15 to 87 min. In the plots, the frequency axis is displayed on a logarithmic scale. For each station, sections of the spectra are shown for overlapping subranges from 15 to 57 min and from 52 to 87 min. The spectral peaks are most pronounced for oscillations with periods of 28, 30.5, 39.5, 43, 43.7, 46.3, 48, 49, 53.7, 68, 72, 73.5, 79, 84.5, and 86.5 min. For individual spectral maxima, Figure 5a,b and Figure 6a,b show the corresponding period values in minutes.

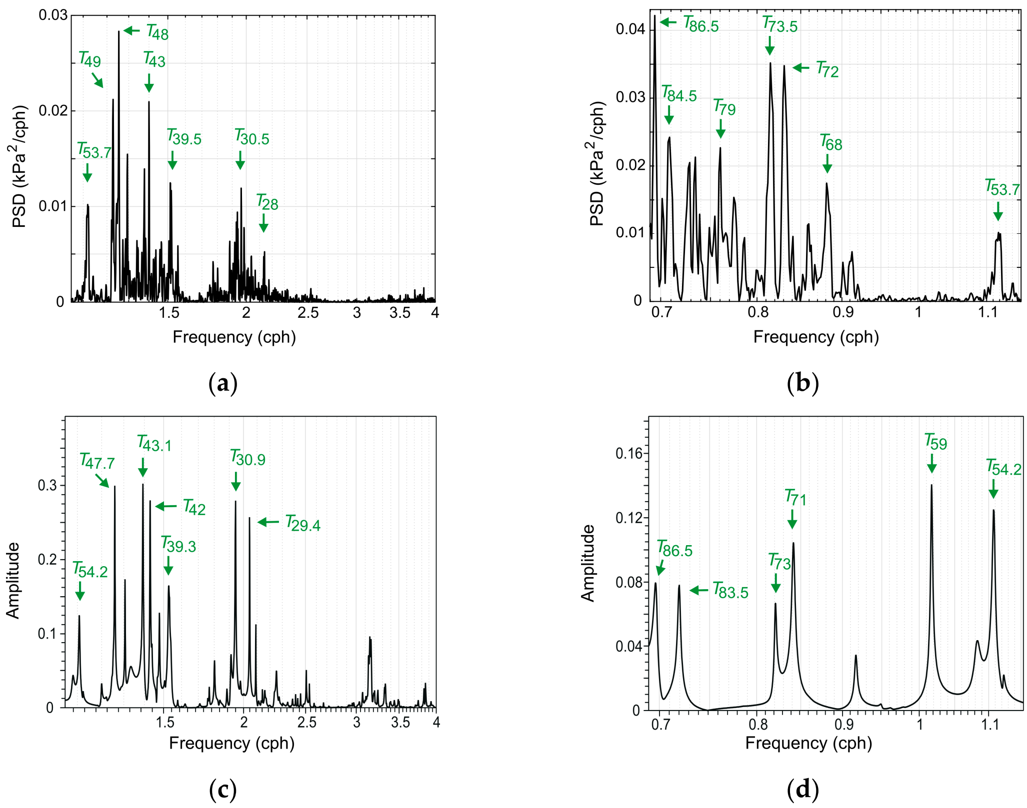

Figure 5. Spectra of oscillations at station PG1 for different ranges of oscillations periods: (**a**) from 15 to 57 min; (**b**) from 52 to 87 min. Resonance curves at model station PG1 for different ranges of oscillation periods: (**c**) from 15 to 57 min; (**d**) from 52 to 87 min.

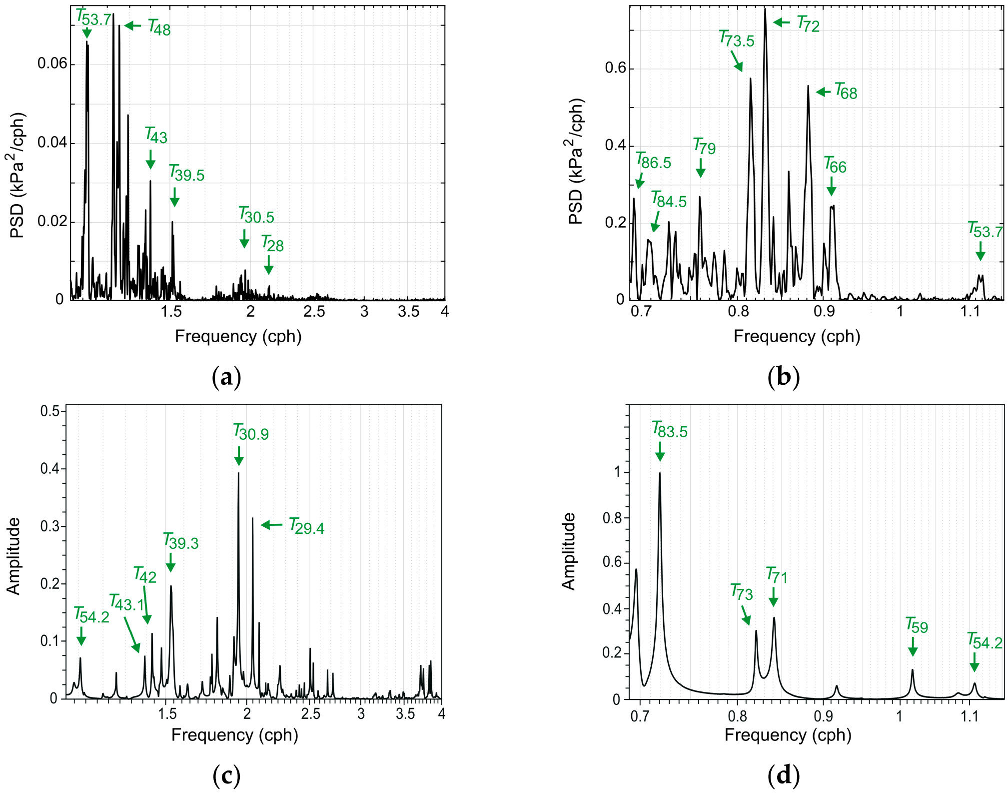

Figure 6. Spectra of oscillations at station PG2 for different ranges of oscillations periods: (**a**) from 15 to 57 min; (**b**) from 52 to 87 min. Resonance curves at model station PG2 for different ranges of oscillation periods: (**c**) from 15 to 57 min; (**d**) from 52 to 87 min.

3.2. Results of Numerical Modeling

At the initial stage of numerical modeling, based on the results of preliminary calculations, the value of the correction to depths is selected. For the main calculation, the value h_{corr} = 1 m is chosen, at which the location of the peaks of the resonance curves approximately corresponds to the location of the peaks of the spectral curves in Figures 5a,b and 6a,b. Figures 5c,d and 6c,d show the resonance curves of the solutions for the model water area for the range of periods from 15 to 87 min. The vertical axis shows the θ_τ maximum values of the amplitude of level oscillations normalized in all directions at points with coordinates of PG1 and PG2. A comparison of Figures 5b,d and 6b,d shows significant differences for periods over 57 min. Groups of spectral maxima correspond to individual maxima on the resonance curves. We believe that these differences are the consequence of the limitation of the applied numerical model, which is local in space. Further, for the model Peter the Great Gulf, we limit the period range under consideration to the upper value of 57 min.

We studied the properties of standing waves in Novik Bay using a numerical model. Figure 7 shows solutions that are characterized by the presence of a nodal line at the entrance to Novik Bay. In the inner part of the bay, during oscillations with periods of 39.3, 29.4, and 18.5 min, there are one, two, and three nodal lines, respectively. The oscillation with period of 86.4 min is the fundamental (Helmholtz) mode for Novik Bay.

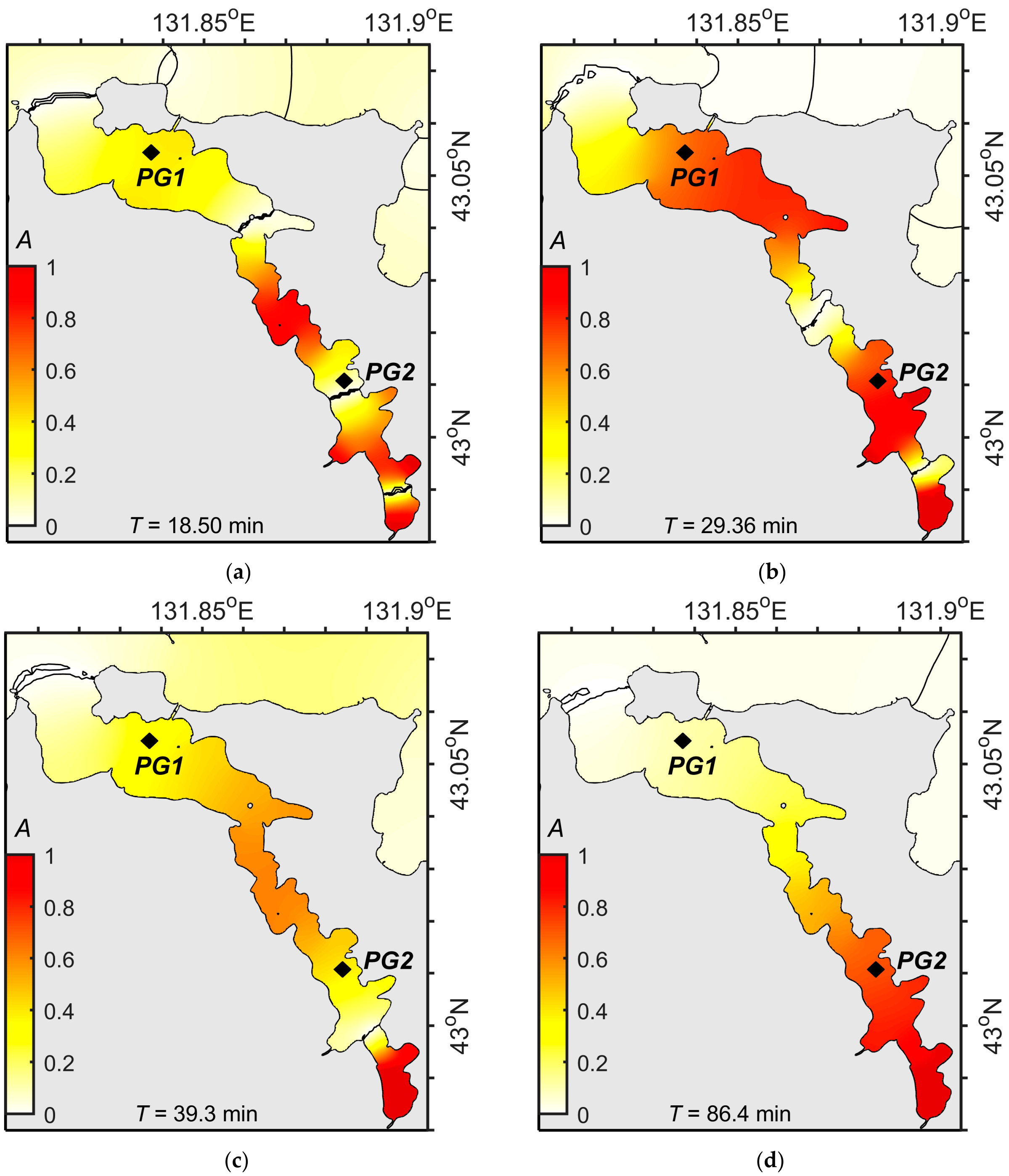

Figure 7. Spatial distributions of the amplitude and phase isolines in Novik Bay for oscillations with periods of (**a**) 18.5, (**b**) 29.4, (**c**) 39.3, and (**d**) 86.4 min. Symbol ♦ shows the position of the autonomous bottom pressure gauges.

Figures 8–10 show the spatial distributions of the amplitude and isolines of the solutions phase with periods corresponding to the maxima on the resonance curves. The solutions were obtained for the north–south direction of the wind forcing ($\theta_\tau = 0$). In Figures 7–10, the phase isolines are shown with step of $\pi/3$. Let us note the specific behavior of phase isolines in the vicinity of nodal lines—the isolines fill some small vicinity of the nodal line. In the calculated value of the phase in the area of nodal lines, characterized by small amplitude values, the contribution of the computational noise of the applied numerical method becomes noticeable.

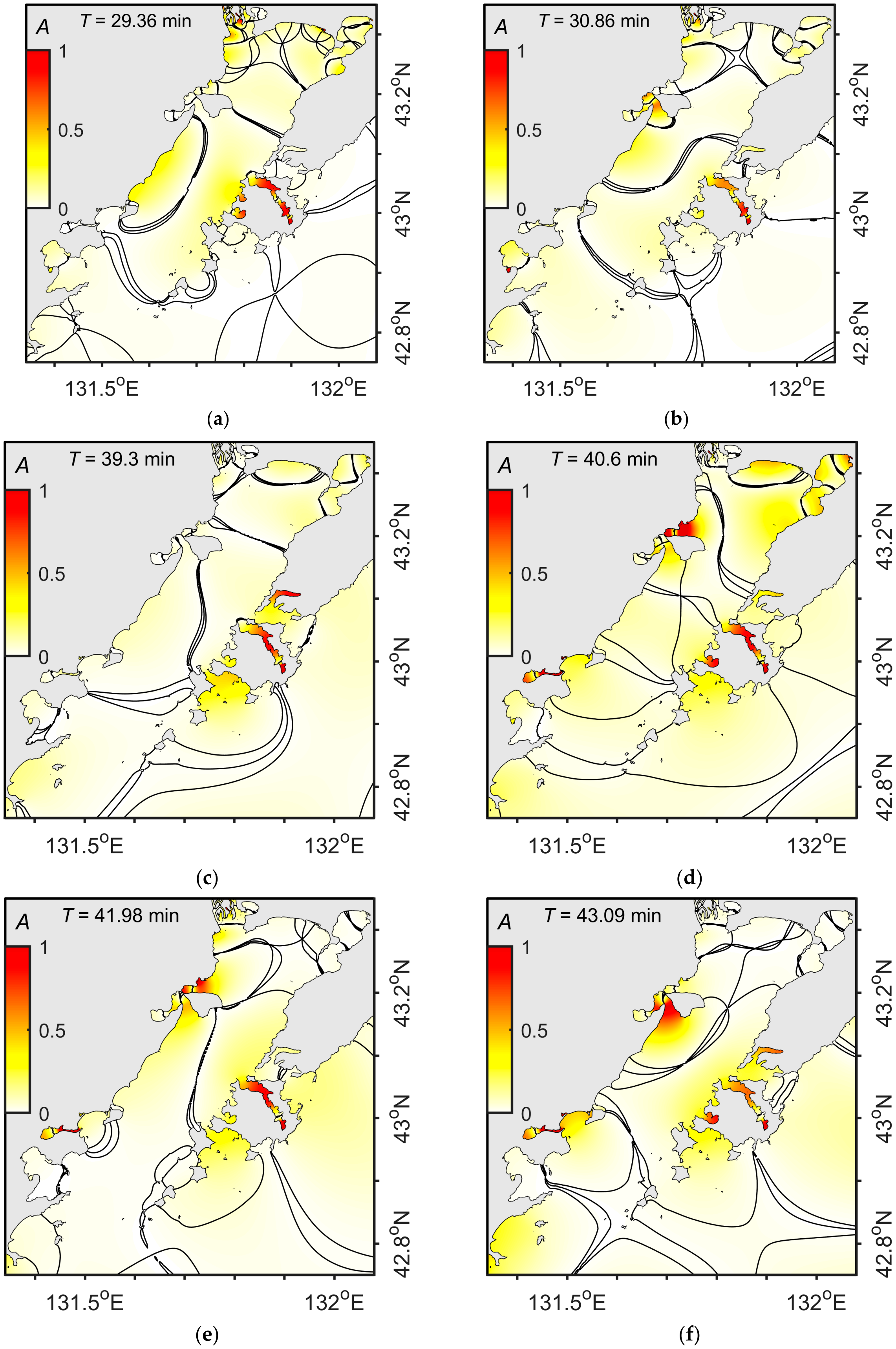

Figure 8. Spatial distributions of the amplitude and phase isolines in Amursky Bay for oscillations with periods of (**a**) 29.4, (**b**) 30.9, (**c**) 39.3, (**d**) 40.6, (**e**) 42, and (**f**) 43.1 min.

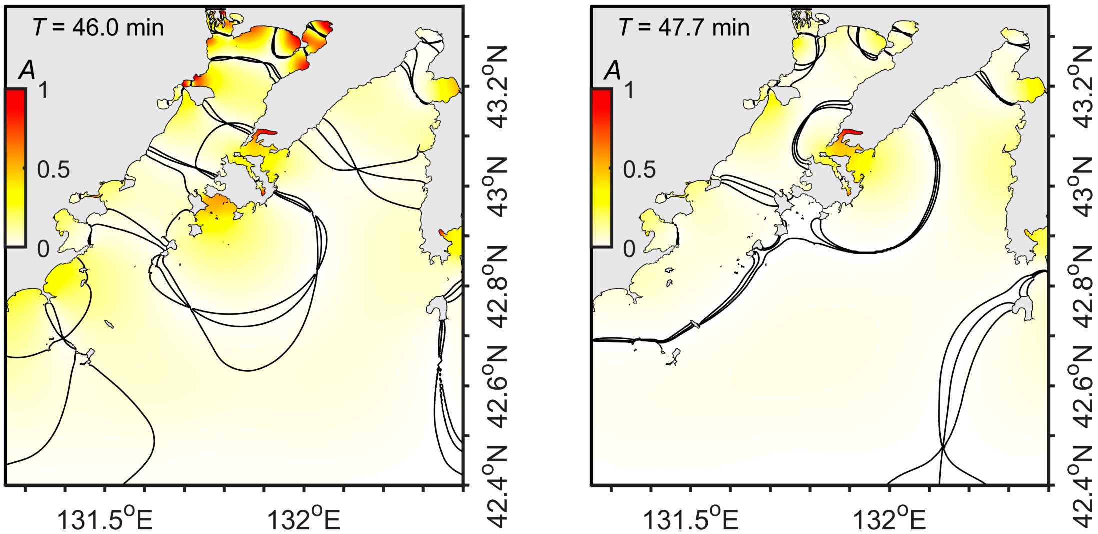

(**a**) (**b**)

Figure 9. Spatial distributions of the amplitude and phase isolines in the northern part of the Peter the Great Gulf shelf for oscillations with periods (**a**) 46 and (**b**) 47.7 min.

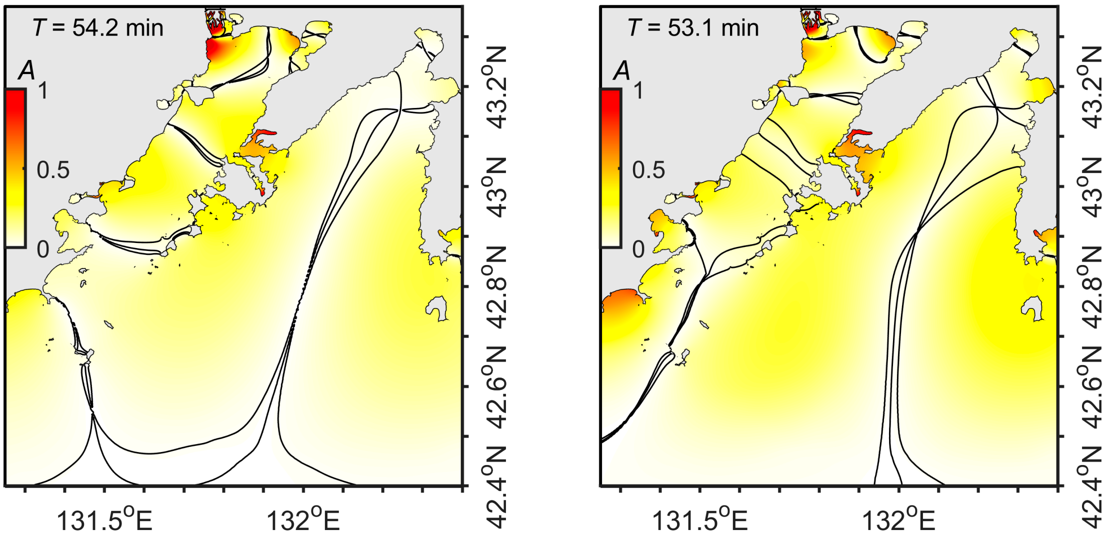

(**a**) (**b**)

Figure 10. Spatial distributions of the amplitude and phase isolines in the northern part of the Peter the Great Gulf shelf (**a**) for the oscillation with a period of 54.2 min and with the main distribution of ice thickness (Figure 4a), and (**b**) for the oscillation with a period of 53.1 min and with the additional variant of ice thickness distribution (Figure 4b).

We believe that in the oscillation with period of 46 min (Figure 9a), the longitudinal oscillations of Amursky and Ussuriysky Bays interact with one of the transverse modes of the Peter the Great Gulf. The wave motion with a period of 47.7 min, shown in Figure 9b, involves the water masses of both Amursky and Ussuriysky Bays, and also the Eastern Bosphorus Strait [14] (p. 176). In this case, one nodal line reaches the middle of Amursky Bay, another one reaches the middle of Ussuriysky Bay.

Figure 10 shows the forms of oscillations with a period of about 54 min obtained at the main and auxiliary configurations of the ice field. In the first case, the maximum on the resonance curve corresponds to the period of 54.2 min; in the second case, to 53.1 min. In addition to the change in the resonant frequency, we also note the strong influence of the ice cover configuration on the structure of the solution in Amursky Bay, especially in its northern part. The resulting solutions are characterized by pronounced manifestation of the transverse mode of the Ussuriysky Bay.

4. Discussion

The use of a local numerical model with extended liquid boundaries imposes corresponding restrictions on the obtained solutions. In this work, in order for the obtained solution to have a physical meaning, transverse oscillations should play the main role in the solution, for example in Amursky and Ussuriysky bays, or local oscillations, for example in the Eastern Bosphorus Strait. The obtained solutions for oscillations with periods less than 55 min satisfy similar restrictions. For numerical study of oscillations with longer periods, it is necessary to include the entire water area of the Sea of Japan in the model and locate the liquid boundaries in the straits or in neighboring water areas. In this case, the grid coverage of the waters of the Peter the Great Gulf will have to be made less detailed due to limited computing resources.

The results presented in Figure 10 demonstrate the strong dependence of the solutions on the configuration of the ice cover in relatively shallow parts of the water area. However, determining the actual thickness of ice can be an extremely difficult task. Apparently, it is necessary to install a distributed system of bottom pressure gauges in order to determine the actual position of the nodal oscillation lines and try to refine the characteristics of the ice cover.

5. Conclusions

To study the features of oscillations in the water column of the Peter the Great Gulf of the Sea of Japan, in situ measurements were carried out on its shelf. The observational data were obtained from two autonomous bottom pressure gauges in Novik Bay in the winter of 2016. The characteristic feature of the energy spectrum, according to the measured data, is the presence of well-defined maxima with periods of 28, 30.5, 39.5, 43, 43.7, 46.3, 48, 49, and 53.7 min. Similar spectral peaks are characteristic of resonant oscillations. In the course of interpretation and joint analysis of the measurements results and simulation, we obtained a series of spatio-temporal parameters for resonant oscillations of the northern part of the Peter the Great Gulf shelf. Calculations of forced oscillations in the form of a response to local periodic wind forcing were carried out using a spectral-difference model that includes the entire water area of the Peter the Great Gulf. The numerical model with difference approximation on the irregular triangular spatial grid is based on the equations of shallow water, taking into account the friction on the bottom and the ice cover. Due to the lack of information on the ice cover configuration, the ice thickness was set by some characteristic values. The location of the peaks on the model resonance curves corresponds to the location of the energy spectrum maxima in in situ measurements data, which indicates the resonant nature of these maxima and the possibility of a significant resonant amplification of level oscillations in the bay by incoming wave packets.

Numerical studies of standing waves' properties in Novik Bay showed that in the inner part of the bay, during oscillations with periods of 39.3, 29.4, and 18.5 min, there are one, two, and three nodal lines, respectively, and one more nodal line is located at the entrance. The oscillation with period of 86.4 min is the fundamental (Helmholtz) mode for Novik Bay.

In further studies of resonant oscillations in the Peter the Great Gulf in winter, it appears advisable to expand the system of gauges in its coastal waters in order to identify the positions of the nodal lines of resonant oscillations. For a numerical study of oscillations with longer periods, it is necessary to include the entire area of the Sea of Japan in the model and locate liquid boundaries in the straits. Detailed information on the distribution and thickness of the ice cover in the waters of the bay is also necessary.

Author Contributions: Conceptualization, S.S., G.D. and I.Y.; methodology, S.S. and I.Y.; software, S.S. and A.P.; validation, S.S. and A.L.; formal analysis, S.S. and A.S. (Alex Shvyrev); investigation and experimental studies, S.S., A.L., A.P. and A.S. (Aleksandr Samchenko); data curation, A.S. (Alex Shvyrev) and A.K.; writing—original draft preparation, S.S.; writing—review and editing, S.S., I.Y., A.L. and A.K.; visualization, S.S., A.S. (Alex Shvyrev) and A.K.; supervision, I.Y. and G.D.; project administration, I.Y. and G.D.; funding acquisition, G.D. All authors have read and agreed to the published version of the manuscript.

Funding: The authors appreciate the support of theoretical studies by the Laboratory of Nonlinear Hydrophysics and Natural Hazards of POI FEB RAS, a project of the Ministry of Science and Education of Russia, project No. 075–15-2022–1127. The experimental studies were carried out as a part of the Russian State assignment on the topic "Study of the fundamental basis of the origin, development, transformation, and interaction of hydroacoustic, hydrophysical, and geophysical fields of the World Ocean" (state number registration: AAAA-A20-120021990003-3).

Institutional Review Board Statement: Not applicable.

Informed Consent Statement: Not applicable.

Data Availability Statement: Experimental data are archived at the Laboratory of Statistical Hydroacoustics (POI FEB RAS), and are available upon request with some restrictions applying to the availability of these data.

Acknowledgments: Numerical results (The State Task for the IACP FEB RAS, No. AAAA-A21-121012290014-3) were obtained with use of IACP FEB RAS Shared Resource Center "Far Eastern Computing Resource" equipment.

Conflicts of Interest: The authors declare no conflict of interest.

References

1. Rabinovich, A.B. Seiches and Harbor oscillations. In *Handbook of Coastal and Ocean Engineering*; Chapter 9; Kim, Y.C., Ed.; World Scientific Publishing: Singapore, 2009; pp. 193–236.
2. Kânoğlu, U.; Okal, E.A.; Baptista, M.A.; Rabinovich, A.B. Introduction to "Sixty Years of Modern Tsunami Science, Volume 1: Lessons and Progress". *Pure Appl. Geophys.* **2021**, *178*, 4689–4695. [CrossRef]
3. Kânoğlu, U.; Rabinovich, A.B.; Okal, E.A.; Pattiaratchi, C.; Baptista, M.A.; Zamora, N.; Catalán, P.A. Introduction to "Sixty Years of Modern Tsunami Science, Volume 2: Challenges". *Pure Appl. Geophys.* **2023**, *180*, 1541–1547. [CrossRef] [PubMed]
4. Vilibić, I.; Rabinovich, A.B.; Anderson, E.J. Special issue on the global perspective on meteotsunami science: Editorial. *Nat. Hazards* **2021**, *106*, 1087–1104. [CrossRef]
5. Defant, A. *Physical Oceanography*; Pergamon Press: London, UK; New York, NY, USA, 1961; Volume 2.
6. Gao, J.; Ji, C.; Liu, Y.; Ma, X.; Gaidai, O. Influence of offshore topography on the amplification of infragravity oscillations within a harbor. *Appl. Ocean Res.* **2017**, *65*, 129–141. [CrossRef]
7. Gao, J.; Zhou, X.; Zang, J.; Chen, Q.; Zhou, L. Influence of offshore fringing reefs on infragravity period oscillations within a harbor. *Ocean Eng.* **2018**, *158*, 286–298. [CrossRef]
8. Medvedev, I.P.; Vilibić, I.; Rabinovich, A.B. Tidal resonance in the Adriatic Sea: Observational evidence. *J. Geophys. Res. Oceans* **2020**, *125*, e2020JC016168. [CrossRef]
9. Polyakova, A.M. *Dangerous and Especially Dangerous Hydrometeorological Phenomena in the North Pacific and Tsunami Waves Near the Primorye Coast*; Dalnauka: Vladivostok, Russia, 2012. (In Russian)
10. Dolgikh, G.I.; Dolgikh, S.G.; Smirnov, S.V.; Chupin, V.A.; Shvets, V.A.; Yakovenko, S.V. Infrasound oscillations in the Sea of Japan. *Dokl. Earth Sci.* **2011**, *441*, 1529–1532. [CrossRef]
11. Smirnov, S.V.; Yaroshchuk, I.O.; Leontyev, A.P.; Shvyrev, A.N.; Pivovarov, A.A.; Samchenko, A.N. Studying resonance oscillations in the eastern part of the Posyet Bay. *Russ. Meteorol. Hydrol.* **2018**, *43*, 88–94. [CrossRef]
12. Smirnov, S.V.; Yaroshchuk, I.O.; Shvyrev, A.N.; Kosheleva, A.V.; Pivovarov, A.A.; Samchenko, A.N. Resonant oscillations in the western part of the Peter the Great Gulf in the Sea of Japan. *Nat. Hazards* **2021**, *106*, 1729–1745. [CrossRef]
13. Chupin, V.; Dolgikh, G.; Dolgikh, S.; Smirnov, S. Study of Free Oscillations of Bays in the Northwestern Part of Posyet Bay. *J. Mar. Sci. Eng.* **2022**, *10*, 1005. [CrossRef]
14. Smirnov, S.V. On calculation of seiche oscillations of the middle part of the Peter the Great Gulf. *Numer. Analys. Appl.* **2014**, *7*, 168–179. [CrossRef]
15. Smirnov, S.V. Seiche Oscillations in the Nakhodka Gulf. *Russ. Meteorol. Hydrol.* **2016**, *41*, 57–62. [CrossRef]
16. Lazaryuk, A.Y.; Kilmatov, T.R.; Marina, E.N.; Kustova, E.V. Seasonal features of the Novik Bay hydrological regime (Russky Island, Peter the Great Bay, Sea of Japan). *Phys. Oceanogr.* **2021**, *28*, 632–646. [CrossRef]

17. Leontyev, A.P.; Yaroshchuk, I.O.; Smirnov, S.V.; Kosheleva, A.V.; Pivovarov, A.A.; Samchenko, A.N.; Shvyrev, A.N. A spatially distributed measuring complex for monitoring hydrophysical processes on the ocean shelf. *Instrum. Exp. Technol.* **2017**, *60*, 130–136. [CrossRef]
18. Thomson, R.E.; Emery, W.J. *Data Analysis Methods in Physical Oceanography*, 3rd ed.; Elsevier Science: New York, NY, USA, 2014; 728p. [CrossRef]
19. Flather, R.A. A numerical model investigation of the storm surge of 31 January and 1 February 1953 in the North Sea. *Quart. J. R. Met. Soc.* **1984**, *110*, 591–612. [CrossRef]
20. Chen, C.; Beardsley, R.; Cowles, G.; Qi, J.; Lai, Z.; Gao, G.; Stuebe, D.; Liu, H.; Xu, Q.; Xue, P.; et al. *An Unstructured Grid, Finite-Volume Community Ocean Model FVCOM User Manual*; SMAST UMASSD Technical Report-13-0701; University of Massachusetts-Dartmouth: North Dartmouth, MA, USA, 2013.
21. Demmel, J.W.; Gilbert, J.R.; Li, X.S. An asynchronous parallel supernodal algorithm for sparse gaussian elimination. *SIAM J. Matrix Anal. Appl.* **1999**, *20*, 915–952. [CrossRef]
22. *Atlas of Peter the Great Gulf and Northwestern Coast of the Sea of Japan to Sokolovskaya Bay (for Small-Size Vessels)*; Gidrograficheskaya Sluzhba KTOF: Vladivostok, Russia, 2003; p. 10. (In Russian)
23. GEBCO Bathymetric Compilation Group. *The GEBCO_2020 Grid—A Continuous Terrain Model of the Global Oceans and Land*; British Oceanographic Data Centre, National Oceanography Centre, NERC: Swindon, UK, 2020. [CrossRef]
24. Mesinger, F.; Arakawa, A. *Numerical Methods Used in Atmospheric Models*; GARP Publication Series No. 17; WMO: Geneva, Switzerland, 1976; p. 64.